POLITECNICO DI TORINO
Repository ISTITUZIONALE

Modeling thermal-fluid-dynamic transients in VIPER cables with OpenSc2

Original
Modeling thermal-fluid-dynamic transients in VIPER cables with OpenSc2 / Placido, D., Riva, N., Salazar, E., Hartwig, Z., Savoldi, L.. - In: IEEE TRANSACTIONS ON APPLIED SUPERCONDUCTIVITY. - ISSN 1051-8223. - (2024), pp. 1-5. [10.1109/tasc.2024.3387880]

Availability:
This version is available at: 11583/2988109 since: 2024-04-26T08:27:27Z

Publisher:
IEEE

Published
DOI:10.1109/tasc.2024.3387880

Terms of use:

This article is made available under terms and conditions as specified in the corresponding bibliographic description in the repository

Publisher copyright

(Article begins on next page)

04 September 2026

This article has been accepted for publication in IEEE Transactions on Applied Superconductivity. This is the author's version which has not been fully edited and content may change prior to final publication. Citation information: DOI 10.1109/TASC.2024.3387880

1PoA03

Modeling thermal-fluid-dynamic transients in VIPER cables with OPENSC^2

Daniele Placido, Nicolò Riva, Erica Salazar, Zachary Hartwig, Laura Savoldi, *member, IEEE*

***Abstract*— In this work, OPENSC^2, a new open-source python-based software for one-dimensional analysis of thermal-hydraulic and electromagnetic transients of superconducting cables is applied to the analysis of thermal-hydraulic transients in a VIPER cable. This is a HTS twisted-stacked cable-in-conduit conductor for fusion machines, and samples were tested at the SULTAN facility in 2019. The OPENSC^2 is calibrated and validated against experiments accounting for the twisting of the tape stacks under the jacket, which is a peculiar feature that needs to be accounted for to properly reproduce the experimental data. The computed results well reproduce the experimental temperature traces in the heated region, paving the way to the use of the same numerical model in the case of winding packs wound with VIPER cables.**

***Index Terms*— Thermal-hydraulic modeling, code validation, HTS stacked-tapes conductors, nuclear fusion.**

I. INTRODUCTION

The most promising candidates to realize a fusion power plant based on the magnetic confinement concept are tokamaks [1] and stellarators [2]. Advantages such as steady-state operations make stellarators very attractive for a low-risk path to a grid-connected fusion reactor, despite the non-planar coil geometry exposes many manufacturing challenges. High-Temperature Superconductor (HTS) stellarator is a desirable choice due to their promising performance at high fields; in tokamaks the CS operating condition can also benefit from the use of HTS coils. Options such as the VIPER cable [3] are currently under consideration. From the architecture point of view, the VIPER cable is an alternative design of the HTS twisted stacked-tape cable (TSTC) concept [4], a declination of the Cable-in-Conduit Conductors design, with the peculiarity of simplifying the configuration and increasing the current density withstood by the cable. One of the main innovations is the exploitation of the vacuum pressure impregnation (VPI) solder process that connects the HTS tapes to each other and to the copper former improving electrical, mechanical, and thermal stability of the cable. As in other cable designs, the stacks of tapes are twisted and transposed for two reasons: to remove strain in the HTS due to fabrication process, and to reduce magnetic flux linkage in the stacks to mitigate transient heat generation during variable magnetic field operating conditions. A 3D CAD of the VIPER cable and its cross section are shown in Fig. 1.

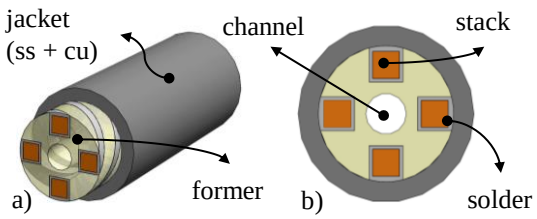

Fig. 1**.** a) 3D CAD drawing of the VIPER cable; b) 2D CAD cross-section of the VIPER cable. The main components labels are also displayed.

It has been already well established [5] that numerical tools are mandatory to analyze the superconducting (SC) coil performances, and a large and interdisciplinary multi-physics and multi-scale approach is beneficial [6]. In the context of SC cable modeling, several tools are available to predict the thermal-hydraulic and electromagnetic behavior of those cables, as well as to give support in their design and characterization. Looking at the field of Low-Temperature Superconductor (LTS) cables for fusion applications, three main tools are well established, namely 4C [7], THEA/SUPERMAGNET [8] and VINCENTA/VENICIA [9], [10]. The above-mentioned tools have two main limitations, namely the proprietary/commercial use and the lack of flexibility. The HTS cables involve new peculiarities, discussed in [11], with the need of dedicating special attention to the gradients building up inside the conductor [12]. A new numerical software (OPENSC^2) has been recently developed at PoliTo for the thermal-hydraulic and electromagnetic 1-dimensional (1D) modeling of SC cables for fusion and power applications. OPENSC^2 is an open-source open-access software, available on GitHub at https://github.com/MAHTEP/OPENSC2, developed exploiting the Object-Oriented Programming (OOP) approach in Python 3 and the Test-Driven Development (TDD) philosophy [13]. The thermal-hydraulic model is discussed in [14], while the electromagnetic model is discussed in [15].

In the framework of a collaboration between MIT and PoliTo, towards the enhancement of the development of open modelling for SC magnets, the analysis of thermal-hydraulic electro-magnetic transients in a non-planar coil of a stellarator wound using the VIPER cable is envisaged with OPENSC^2. As a first step of the overarching activity, the main aim of the work here presented is the first thermal-hydraulic validation OPENSC^2 against experimental results performed at the SULTAN test facility on VIPER-like samples.

Daniele Placido and Laura Savoldi are with Dipartimento Energia "Galileo Ferraris", Politecnico di Torino, Torino, I-10129 Italy (e-mail: daniele.placido@polito.it, laura.savoldi@polito.it).
Nicolò Riva and Zachary Hartwig are with PFSC, Massachusetts Institute of Technology, Boston, Massachusetts (nico.riva@mit.edu, hartwig@psfc.mit.edu,)
Erica Salazar is with Commonwealth Fusion Systems, Devens, Massachusetts (ericasal@mit.edu)

Color versions of one or more of the figures in this article are available online at http://ieeexplore.ieee.org

This work is licensed under a Creative Commons Attribution 4.0 License. For more information, see https://creativecommons.org/licenses/by/4.0/

This article has been accepted for publication in IEEE Transactions on Applied Superconductivity. This is the author's version which has not been fully edited and content may change prior to final publication. Citation information: DOI 10.1109/TASC.2024.3387880

II. Experimental Setup

The SULTAN test facility is well established to test SC cable design from all around the world [16]. The measurements considered in this paper are the ones obtained in the SULTAN Delta test in 2019. The sample is composed of two legs of length 2.8 m joined at their lower ends by means of a 400 mm length low resistance joint, called respectively Alpaca and Bison. The VIPER cable of each leg is composed of four HTS tape stacks, each of which is composed of 50 tapes of 87 μm thick and 4 mm wide crafted by SuperOx. The stacks are arranged in a cross pattern, and each stack is orthogonal to the stack next to it. These are housed within rectangular channels obtained by continuous extrusion on the outer perimeter of the copper core and provided with a pitch of 200 mm. Cooling is ensured by the flow of supercritical helium (SHe) in the central 5 mm diameter channel, which is characterized by a low hydraulic impedance. This rather compact structure is enclosed in a hollow copper cylinder, which is itself contained into a stainless-steel jacket, with outer diameter of 27.7 mm, which provides mechanical stability to the cable. Each leg is cooled by SHe at 1 MPa; inlet mass flow rate and temperature can be tuned respectively in the ranges [0, 10.0] g/s and [4.5, 60.0] K.

TABLE I
SULTAN INSTRUMENTATION TYPE, AXIAL COORDINATES AND NOMENCLATURE FOR THE RIGHT LEG (BISON)

Name	Type	#	Coordinate (m)	Nomenclature
T2	Cernox	3	0.16	T21 T22 T23
TH6	Cernox	2	0.56	TH61 TH62
H2	Heater	1	0.56	H2
H4	Heater	1	0.71	H4
T4	Cernox	3	0.96	T41 T42 T43

The SULTAN facility has many sensors for cable diagnostics, among which flow meters, temperature sensors and heaters. Each leg is provided with two surface quench resistive heaters, one of which is in the center of the high magnetic field zone while the other is placed downstream to give additional heat. Temperature is measured with Cernox-type temperature sensors and namely, for each leg, two sensors at the same axial location of the primary heater but at different azimuthal positions, three Cernox upstream and downstream the high field region and four sensors at the inlet and at the outlet of the cable. Table I summarizes the axial locations of heaters and sensors, introducing the nomenclature, while Fig. 2 shows a schematic representation of the SULTAN experimental set up.

The case study here is the shot Delta1C030604 which had the aim of checking the instrumentation without current and magnetic field. A flow rate of 3 g/s of SHe at 1 MPa and 4.5 K flows in both legs, while the surface heater H2 on the right leg of the sample is activated for approximately 1.1 s depositing 32 W of heat power in the middle of the high magnetic field region on a length of ~1 cm.

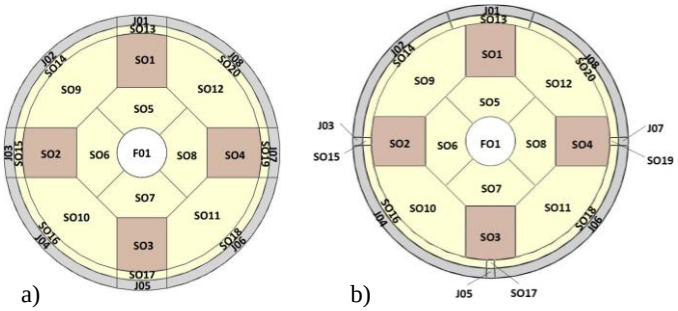

Fig. 3. Cross-section discretization and naming scheme associated to Γ_1 (a) and Γ_2 (b).

III. Simulation Setup in OpenSC2

In OpenSC^2, the thermal-hydraulic model accounts for the Euler-like equations for the fluids written in the non-conservative variables pressure, temperature, and velocity and the 1D time dependent heat equation for the solids. The main issue while dealing with design of cables which have a bulky stabilizer (former) is the discretization of the cross section in sub regions, that in OpenSC^2 become the conductor components. Several cross-section discretizations were considered; for the sake of conciseness, this paper focuses on two of them, referred to as Γ_1 and Γ_2 below.

Fig. 3 presents the cross-section discretizations used in this paper and introduces the subcomponents naming scheme. In Γ_1 each HTS stack is modeled as a mixed Strand Object (SO) which also includes the solder. For the sake of simplicity, the material was treated as copper apart from the superconducting layer. This approximation overestimates the thermal conductivity and underestimates the heat capacity. The two effects tend to cancel out because even though the component has a greater temperature rise due to the lower heat capacity, the heat conduction in the solid is enhanced by the higher conductivity. The stabilizer is composed in a radial fashion, into eight subcomponents, namely four equivalent inner regions around the central channel and four equivalent outer regions between the stacks of tapes. The discretization of the copper hollow cylinder and of the stainless-steel jacket is shown in Fig 3a. Finally, the central channel is modeled as a single fluid component object.

In Γ_2, the discretization of the VIPER inner region (central channel, stacks of tapes and former) is the same as in Γ_1 (Fig 3b). The discretization of the copper hollow cylinder and of the outer jacket, should allow modelling the actual location of the heaters and Cernox, avoiding temperature homogenization errors. A radial and consistent discretization of the two hollow cylinders was then selected. A summary of the cross section of the representative components used for Γ_1 and Γ_2 is reported in Table II.

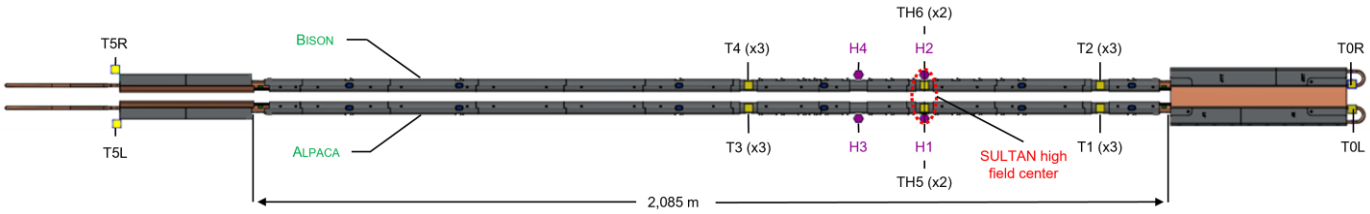

Fig. 2. Sketch of the Delta sample at SULTAN test facility, diagnostic locations, and computational domain.

This work is licensed under a Creative Commons Attribution 4.0 License. For more information, see https://creativecommons.org/licenses/by/4.0/

This article has been accepted for publication in IEEE Transactions on Applied Superconductivity. This is the author's version which has not been fully edited and content may change prior to final publication. Citation information: DOI 10.1109/TASC.2024.3387880

TABLE II
REPRESENTATIVE CONDUCTOR COMPONENT CROSS-SECTION IN mm^2 FOR DISCRETIZATION Γ_1 AND Γ_2

Name	Γ_1	Γ_2
FO1	19.6	19.6
JO1	5.10	10.9
JO3		0.85
JO2	12.1	15.1
JO4		20.1
SO1	27.1	27.1
SO5	9.97	9.97
SO9	29.3	29.3
SO13	4.27	8.62
SO15		0.67
SO14	8.93	11.9
SO16		15.9

Note that since the internal components of the Delta cable are twisted, no symmetry is present in the cable. Moreover, because the copper hollow cylinder is straight, the rotation of the inner solid components around the central channel leads to variable contact perimeters $P(\tau)$ and variable conductive heat transfer coefficients (HTC) between the inner solid components and the hollow copper cylinder. Fig. 4 illustrates these issues for components SO1 and SO13.

To take this effect into account, $P(\tau)$ is assigned as a piecewise linear function of τ, where τ is the rotation angle of the cross section with respect to its original position, which for the present case coincides with what is shown in Fig.3 b). For the components SO1 and SO13, Eq. 1 holds:

$$P(\tau) = \begin{cases} r\,\alpha_2, \;\; \tau \in \left[0, \dfrac{\alpha_1-\alpha_2}{2}\right) \cup \tau \in \left[2\pi - \dfrac{\alpha_1-\alpha_2}{2}, 2\pi\right) \\ r\left(\dfrac{\alpha_1-\alpha_2}{2} - \tau\right), \;\; \tau \in \left[\dfrac{\alpha_1-\alpha_2}{2}, \dfrac{\alpha_1+\alpha_2}{2}\right) \\ r\left[\tau - \left(2\pi - \dfrac{\alpha_1+\alpha_2}{2}\right)\right], \;\; \tau \in \left[\dfrac{\alpha_1+\alpha_2}{2}, 2\pi - \dfrac{\alpha_1-\alpha_2}{2}\right) \end{cases} \quad 1)$$

where r is the distance of the contact interface from the center of the channel in m and α_1 and α_2 are the angles subtended to components SO13 and SO1 respectively (in rad).

Regarding the HTC, it is based on the evaluation of the distance between the barycenter of the components as a function of τ as shown in Eq. 2

$$htc(\tau) = \left[\frac{s_{SO1}(\tau)}{k_{SO1}(T,B)} + \frac{s_{SO13}(\tau)}{k_{SO13}(T,B)} + R_c\right]^{-1} \quad 2)$$

where $s_{SO1}(\tau)$ and $s_{SO13}(\tau)$ are the variable thickness of the components in m, $k_{SO1}(T,B)$ and $k_{SO13}(T,B)$ are the thermal conductivity of the material as function of temperature (and eventually of the magnetic field) in W/m/K, while R_c is the contact thermal resistance in m^2K/W. A summary of the contact perimeters and HTC between solid components for both configurations is given in Table III. Only a representative subset of the interfaces is shown, the others can be obtained by symmetry consideration.

For modeling purposes, both the cable-to-cable and the upper joints were neglected, as shown in Fig. 2. Fluid friction factor coefficient and convective HTC are evaluated by means of well-established empirical correlations, respectively Colebrook and Dittus-Boelter.

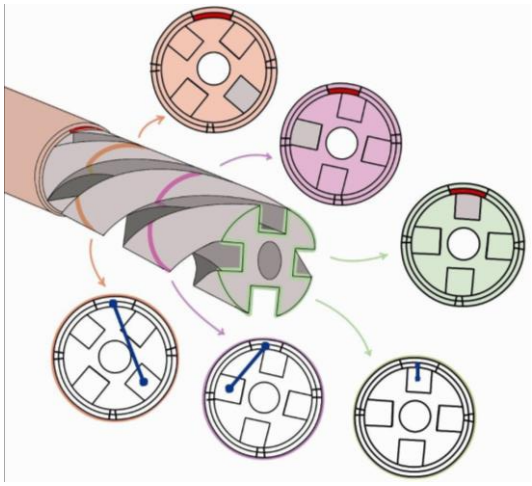

Fig. 4. Schematization (top) of the variable contact perimeter between the heated component (SO13) and one of the stacks of tapes (SO1) (Note that there are angular locations where the components are not in contact), and (bottom) of the variable conductive HTC based on the distance between the barycenter of the components.

TABLE III
REPRESENTATIVE CONTACT PERIMETERS (P) IN mm AND HEAT TRANSFER COEFFICIENTS (HTC) IN $Wm^{-2}K^{-1}$ BETWEEN CONDUCTOR COMPONENTS FOR Γ_1 AND Γ_2 CONFIGURATIONS

Interface	P_{Γ_1}	P_{Γ_2}	HTC
FO1-SO5	3.93	3.93	Dittus-Boelter
SO1-SO5	5.0	5.0	
SO1-SO9	5.2	5.2	500
SO1-SO13	5.0	$P(\tau)$	
SO5-SO6	2.1	2.1	
SO5-SO9	1.1	1.1	10^4
SO9-SO14	10.0	$P(\tau)$	
SO13-SO14	0.87	0.85	
SO13-JO1	5.5	8.3	
SO14-JO2	11.2	15.6	
SO15-JO3	5.5	0.82	10^2
SO16-JO4	11.2	19.4	
SO17-JO5	5.5	0.82	
JO1-JO2	1.03	1.0	10^3

It is worth remarking that simulations carried out with Γ_1 do not exploit the newly introduced feature of the variable $P(\tau)$, as opposed to simulations performed with Γ_2; however, both models share the same set of conductive HTCs, collected in Table III, obtained after a proper calibration.

.IV. THERMAL HYDRAULIC VALIDATION

The results computed with both models Γ_1 and Γ_2 are compared to the measurements in Fig. 5, that shows the temperature time evolutions in the heated region (high magnetic field zone) as well as upstream and downstream this region. Measurements from Cernox T22 and T41 are not shown because they exhibit respectively 60.0% and 53.1% relative error compared to the other T2 and T4 sensors. For both models, the computed temperature shown in Fig 5 is the average, weighted on the heat capacities per unit length ($C = A\rho c_p$), of the stabilizer and jacket temperature (named *AO*), where A is

This work is licensed under a Creative Commons Attribution 4.0 License. For more information, see https://creativecommons.org/licenses/by/4.0/

This article has been accepted for publication in IEEE Transactions on Applied Superconductivity. This is the author's version which has not been fully edited and content may change prior to final publication. Citation information: DOI 10.1109/TASC.2024.3387880

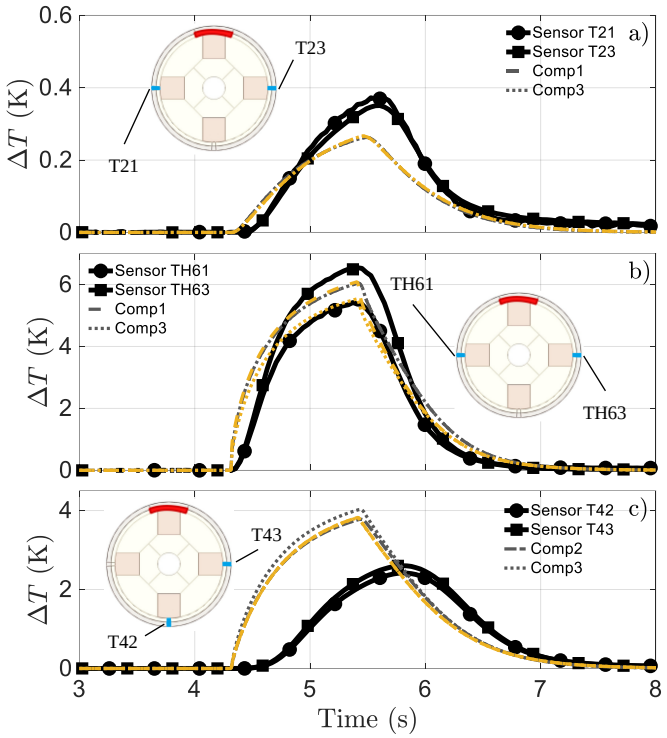

Fig. 5. Temperature time evolution for simulation performed with Γ_1 and Γ_2. a) upstream of the heated region; b) in the heated region; c) downstream of the heated region. Gray lines Γ_1, yellow lines Γ_2. In the insets the location of the temperature sensors is shown, while the red arches identify the heated component (Comp1 = $\boldsymbol{AO_{15,3}}$; Comp2 = $\boldsymbol{AO_{17,5}}$; Comp3 = $\boldsymbol{AO_{19,7}}$).

the component cross section, while ρ and c_p are respectively material density and specific heat. This is done to consider that the Cernox were placed on the hollow copper cylinder but anchored to the jacket. The jacket, in this scenario, is not in perfect thermal equilibrium with the copper due to a clearance in tolerances between these components, which is not compensated by the Lorentz force arising by the application of a current and a magnetic field.

From the qualitative point of view, the numerical simulations carried out with both models reproduce all the main features of the physics of the problem and namely: 1) backward heat diffusion due to conduction in solid components, 2) localized heating up when the surface heater is on and 3) subsequent cooling down when it is switched off, as well as 4) advection/diffusion of heat in the region downstream the heater due to conduction in the solid component and convection in the coolant. Moreover, they qualitatively reproduce the temperature distribution on the cable cross section at different axial coordinates, and, consistently with the flow measurements, the model does not compute any backflow. In the heated region, the difference between the calculated temperatures for the average objects (AO) $AO_{15,3}$ and $AO_{17,5}$ is close to the difference between the measured temperatures; in the upstream and downstream regions, a higher temperature uniformity is both measured and computed. A first order motivation is that in those regions no heat is deposited. Moreover, for the upstream region, it should be considered that the sensors are closer to the inlet than to the heated region, so the temperature here is still uniform. In the downstream region, heat is transported by diffusion and advection. Temperature gradients in the cross section are smeared out by both the high value of the HTC and the twist pitch of the stacks, which contributes to temperature homogenization. In the upstream region, the difference between measured and computed values is comparable with the accuracy of the software (~0.1 K) for both configurations. In the heated region both Γ_1 and Γ_2 show acceptable relative errors of 12% and 7% respectively. From Fig. 5c, downstream region, it can be argued that the computed values overestimate the measured one; relative errors for Γ_1 and Γ_2 are respectively ~65 % and ~55%. A possible explanation, to be further investigated, could be a combination of model side temperature overestimation due to the choice of the fixed values adopted for the HTC, and poor Cernox accuracy from the experimental point of view, due to the lack of Lorentz force. One of the most striking features in Fig. 5c, common to both cable models, is that in OpenSc^2 the advective phenomenon is detected ~0.3 s earlier than the experimental data. Indeed, the computed fluid velocity in the heated region at the beginning of the heating is ~1 m/s; since the distance between Cernox TH6 and Cernox T4 is 0.4 m, the expected propagation time of the heat is ~0.4 s, in quite good agreement with the experimental measurements.

V. Conclusions and Perspective

In this work the validation of the thermal-hydraulic model of OpenSc^2 against experimental measurements carried out on VIPER Delta cable at SULTAN in 2019. Two models with two different cross section discretization were discussed, and the main results compared to the measured temperature time evolutions. The evidence from this study confirms the capability of the tool to model several cable configurations and topologies. These results suggest that OpenSc^2 can reproduce, at least qualitatively, the main thermal-hydraulic phenomena that characterize the propagation of a heat slug (local heating, small propagation upstream of the heated zone, stronger propagation downstream). From a quantitative point of view, although good agreement was obtained in the upstream and heated regions, both models were found to overestimate the experimental measurements in the downstream region. Further investigation on the choice of heat transfer coefficients through a detailed sensitivity study will be carried out to clarify this point.

Overall, the configuration with a more realistic azimuthal representation of the heated zone (Γ_2) was found to perform better than the one with a more averaged approach for jacket (Γ_1). However, further validation under the scenario of a quench propagation is mandatory to finally assess both the thermal-hydraulic and the electromagnetic models in the software.

Future work will explore the possibilities of implementing the multiconductor module, suitable for dealing with winding packs in fusion reactors, and a preliminary study of a Stellarator non-planar coil.

Acknowledgment

This research benefited from a COST-Action short term student mission grant, whereby Dr. Placido was able to meet and discuss in person with Dr. Riva and Prof. Hartwig at MIT.
Support was given by Commonwealth Fusion Systems and PSFC MIT via RPP27.

This work is licensed under a Creative Commons Attribution 4.0 License. For more information, see https://creativecommons.org/licenses/by/4.0/

This article has been accepted for publication in IEEE Transactions on Applied Superconductivity. This is the author's version which has not been fully edited and content may change prior to final publication. Citation information: DOI 10.1109/TASC.2024.3387880

REFERENCES

[1] T. Donné, "European Research Roadmap to the Realisation of Fusion Energy," *EUROfusion*, 2018 [Online]. Available: https://euro-fusion.org/eurofusion/roadmap/.

[2] J. L. Johnson, "Stellarator and Heliotron Devices," *Nucl. Fusion*, 1999, doi: 10.1088/0029-5515/39/2/701.

[3] Z. S. Hartwig *et al.*, "VIPER: an industrially scalable high-current high-temperature superconductor cable," *Supercond. Sci. Technol.*, vol. 33, no. 11, p. 11LT01, Oct. 2020, doi: 10.1088/1361-6668/abb8c0.

[4] C. Barth, M. Takayasu, N. Bagrets, C. M. Bayer, K.-P. Weiss, and C. Lange, "Temperature-and field dependent characterization of a twisted stacked-tape cable," *Supercond. Sci. Technol.*, vol. 28, no. 4, p. 45015, Feb. 2015, doi: 10.1088/0953-2048/28/4/045015.

[5] R. Zanino and L. S. Richard, "Multiscale approach and role of validation in the thermal-hydraulic modeling of the ITER superconducting magnets," *IEEE Trans. Appl. Supercond.*, vol. 23, no. 3, 2013, doi: 10.1109/TASC.2012.2236134.

[6] R. Zanino, D. Ciazynski, N. Mitchell, and L. S. Richard, "Coupled mechanical–electromagnetic–thermal–hydraulic effects in Nb3Sn cable-in-conduit conductors for ITER," *Supercond. Sci. Technol.*, vol. 18, no. 12, p. S376, Nov. 2005, doi: 10.1088/0953-2048/18/12/026.

[7] L. Savoldi Richard, F. Casella, B. Fiori, and R. Zanino, "The 4C code for the cryogenic circuit conductor and coil modeling in ITER," *Cryogenics (Guildf).*, 2010, doi: 10.1016/j.cryogenics.2009.07.008.

[8] M. Bagnasco, D. Bessette, L. Bottura, C. Marinucci, and C. Rosso, "Progress in the integrated simulation of thermal-hydraulic operation of the ITER magnet system," 2010, doi: 10.1109/TASC.2010.2043836.

[9] D. Bessette, N. Shatil, and E. Zapretilina, "Simulations of the ITER toroidal field coil operation with the VINCENTA code," 2006, doi: 10.1109/TASC.2006.873258.

[10] V. Amoskov *et al.*, "Validation of VINCENTA modelling based on an experiment with the central solenoid model coil of the international thermonuclear experimental reactor," *Plasma Devices Oper.*, 2006, doi: 10.1080/10519990500518001.

[11] A. Zappatore, W. H. Fietz, R. Heller, L. Savoldi, M. J. Wolf, and R. Zanino, "A critical assessment of thermal–hydraulic modeling of HTS twisted-stacked-tape cable conductors for fusion applications," *Supercond. Sci. Technol.*, vol. 32, no. 8, p. 084004, Jul. 2019, doi: 10.1088/1361-6668/AB20A9.

[12] A. Zappatore, W. H. Fietz, R. Heller, L. Savoldi, M. J. Wolf, and R. Zanino, "A critical assessment of thermal–hydraulic modeling of HTS twisted-stacked-tape cable conductors for fusion applications," *Supercond. Sci. Technol.*, Aug. 2019, doi: 10.1088/1361-6668/ab20a9.

[13] K. Beck, "Test-driven development : by example," p. 220, 2003, Accessed: C. 02, 2021. [Online]. Available: https://www.oreilly.com/library/view/test-driven-development/0321146530/.

[14] L. Savoldi, D. Placido, and S. Viarengo, "Thermal-hydraulic analysis of SuperConducting cables for energy applications iwth a novel open object-oriented software: OPENSC2," *Cryogenics (Guildf).*, vol. 124, p. 103457, 2022.

[15] S. Viarengo, F. Freschi, D. Placido, and L. Savoldi, "Current distribution modeling in the open-source OPENSC2 tool for the multi-physics analysis of HTS and LTS superconducting cables," *IEEE Trans. Appl. Supercond. Submitt. to*, 2021.

[16] P. Bruzzone *et al.*, "Upgrade of operating range for SULTAN test facility," *IEEE Trans. Appl. Supercond.*, vol. 12, no. 1, pp. 520–523, 2002, doi: 10.1109/TASC.2002.1018457.

This work is licensed under a Creative Commons Attribution 4.0 License. For more information, see https://creativecommons.org/licenses/by/4.0/